pH-dependent conductance behaviors of layer-by-layer self-assembled carboxylated carbon nanotube multilayer thin-film sensors

Dongjin Lee, and Tianhong Cui

Citation: Journal of Vacuum Science & Technology B: Microelectronics and Nanometer Structures Processing, Measurement, and Phenomena **27**, 842 (2009); doi: 10.1116/1.3002386

View online: https://doi.org/10.1116/1.3002386

View Table of Contents: https://avs.scitation.org/toc/jvn/27/2

Published by the American Institute of Physics

*p*H-dependent conductance behaviors of layer-by-layer self-assembled carboxylated carbon nanotube multilayer thin-film sensors

Dongjin Lee and Tianhong Cui[a)]
Department of Mechanical Engineering, University of Minnesota, Minneapolis, Minnesota 55455

(Received 13 August 2008; accepted 15 September 2008; published 30 March 2009)

The authors report *p*H-dependent conductance behaviors of single-walled carbon nanotube (SWCNT) multilayer thin-film sensors. SWCNTs are functionalized with carboxylic groups, and layer-by-layer assembled alternatively with polycation, polydiallyldimethyammonium chloride on the microfabricated metal electrodes. Current-voltage (*I-V*) characteristics show that the conductance of SWCNT multilayer thin-film sensors decreases with increase of *p*H values. On the other hand, the multilayer resistors with polymethylmethacrylate (PMMA) as a passivation layer demonstrate the increasing conductance with *p*H, opposite to the case of the absence of PMMA layer. The conductance change in the absence of PMMA attributes to doping/undoping of holes as charge carriers by molecular protonation/deprotonation of *p*-type semiconducting SWCNTs. With PMMA layer, concentration gradient of hydrogen ions on the dielectric forms the gate bias voltage, which changes the conductance of underlying semiconducting SWCNT layer. Each *p*H-dependent behavior has versatile applications for chemical and biological detections. © *2009 American Vacuum Society.* [DOI: 10.1116/1.3002386]

I. INTRODUCTION

The carbon nanotube (CNT) has been receiving a great attention in many research fields as a versatile functional material for past 2 decades due to the extraordinary mechanical, optical, and electrical properties with the excellent chemical and thermal stability.[1] To exploit these endowed properties, lots of effort has been made with the emphasis on the incorporation of CNTs to electronic devices[2] and electromechanical systems[3] as a basic building block. Due to the dual electronic properties, semiconducting or metallic relying on the chirality and diameter,[1] CNTs are specifically applicable to nanoelectronic devices, where semiconducting and metallic CNTs play roles of channel material and conductive interconnect, respectively.[4] As an advantage of using CNTs as a semiconducting material in field effect transistors (FETs), CNTs revealed higher charge carrier mobility than silicon based devices.[5] In conjunction with the mechanical property, CNTs have been used as building blocks in the nanoelectromechanical switch and detector for nanoscale motion.[6]

Another mainstream of CNT applications includes chemical and biological sensors to take advantage of the sensitive electrochemical reaction in surface atoms or functional blocks along with chemical stability as aforementioned. The study of electrochemical properties[7] leads to significant biosensing applications, capable of detecting or monitoring specific biomolecules for the diagnostic as well as therapeutic purpose. CNT-based biosensors detected protein,[8] DNA,[9] immunoglobulin,[10] neurotransmitters,[11] and other important biomolecules[12] from the physiological aspect in the presence and absence of bioreceptors. Among extensive chemical and biological applications, *p*H sensing is of great importance in scientific research and clinics since it plays a key role in biochemical systems, where the solubility, charge of biomolecules, and equilibrium of the biochemical reactions are immensely affected by *p*H. As a particular example, cancer cells tend to breed in the acidic environment (~*p*H 6.5), whereas normal human blood has *p*H value of 7.35, which slightly decreases to 7.2 by the intake of food.[13] In consequence, *p*H detection and monitoring provides meaningful health information. Furthermore, there are many biochemical reactions accompanying *p*H changes by which the concentration of target biomolecules can be traced for biosensing applications.

Combined with extremely sensitive electronic properties of SWCNTs, *p*H sensors have recently been reported.[14,15] Although the *p*H sensing mechanism has been generally known to be protonation, it has been interpreted in different ways.[14] Our group has been working on *p*H sensors using nanoparticles and CNTs. We showed layer-by-layer (LbL) self-assembled nanoparticle and CNT had the *p*H sensing capability with high sensitivity and fast response.[16] However, their sensing mechanism has not been clearly understood. In this report, we present two different types of *p*H-dependent conductance behaviors of LbL self-assembled polyelectrolyte and SWCNT multilayer thin-film sensors. More importantly, the *p*H sensing mechanism of LbL film is clearly explained from the semiconductor perspective. The functionalized SWCNTs (f-SWCNTs) are assembled alternately with polycation onto microfabricated electrodes on the silicon/silicon dioxide substrate with and without polymethyl methacrylate (PMMA) as an isolation for transducing SWCNT. The fabricated SWCNT sensors showed completely different *p*H responses from the reports[14,15] by using carboxyl group f-SWCNTs and a dielectric for the isolation of semiconducting SWCNTs.

[a)]Author to whom correspondence should be addressed; electronic mail: tcui@me.umn.edu

II. EXPERIMENT

A. Chemical functionalization of SWCNT

SWCNTs (1–2 nm in diameter and 50 μm in length) were chemically functionalized in 3:1 mixture of concentrated sulfuric (H_2SO_4) and nitric acid (HNO_3) at 110 °C for an hour, followed by vacuum filtering with the pore size of 0.22 μm to remove soot, metallic particles, and shorter CNTs. After rinsing with de-ionized water (DIH_2O) several times until *p*H approached 5, f-SWCNTs were harvested and dispersed into fresh DIH_2O with the aid of ultrasonication for an hour. Subsequently, the SWCNT solution was centrifugated at a speed of 5000 rpm (4500 g, Eppendorf centrifuge 5804) for 20 min to eliminate longer SWCNTs, aggregates, and bundles. By the end, the supernatant was carefully decanted and the precipitation was abandoned. f-SWCNTs were dispersed well and had great stability due to induced hydrophilic functional groups on the surface of SWCNTs. In order to determine the final concentration, 500 μl of SWCNT solution was dropped onto a glass slide, and weight was measured after evaporation. The final concentration of SWCNT solution was about 0.06 wt %.

B. Fabrication of SWCNT multilayer sensors

A silicon (Si) wafer with thermally grown silicon dioxide (SiO_2) 2 μm thick was cleaned in a piranha solution (3:1 H_2SO_4:H_2O_2) at 120 °C for 15 min, and rinsed with a copious amount of DIH_2O. Chromium (Cr, 100 nm) and gold (Au, 200 nm) were electron-beam evaporated for electrode materials, and patterned as source-drain electrodes using photolithography. Next, a lift-off process was used to fabricate the opening window for the adsorption of SWCNT multilayer to the channel area, eliminating a possible direct electrochemical reaction between *p*H buffer solution and Cr/Au electrode covered with SWCNT multilayer. After developing photoresist, oxygen (O_2) plasma was used to remove the residual photoresist completely in the opening window at a power of 100 W for 1 min with O_2 flow rate of 100 SCCM (SCCM denotes cubic centimeter per minute at STP), and this is also to change the surface hydrophilic, which is crucial to the subsequent LbL assembly. Polyelectrolytes used for LbL assembly as a polycation and polyanion were 1.4 wt % polydiallyldimethyammonium chloride (PDDA) and 0.3 wt % sodium polystylenesulfonate (PSS) with 0.5*M* sodium chloride (NaCl), respectively. The precursor layer of $(PDDA/PSS)_2$ was self-assembled on the opening window near channel area for the charge enhancement, followed by the assembly of $(PDDA/SWCNT)_5$ for the electrochemical transducer layer. The dipping times used for polyelectrolytes and SWCNTs were 10 and 15 min, respectively. PMMA was spun to yield 300 nm thickness on the SWCNT thin-film sensors to compare results of devices with and without PMMA as a dielectric layer.

C. Electronic characterization

Two types of electronic characterizations were used: current-voltage (*I-V*) measurement at the steady state and dynamic responses at the transient state using data logging system. *I-V* characteristics was measured using semiconductor parameter analyzer (HP 4156A) at different *p*H buffer solutions (mixture of NaH_2PO_4 and Na_2HPO_4 with the buffer strength of 80 mM), in the range of biochemical reactions. After adding each *p*H buffer solution, 1 min is allowed to reach the steady state followed by the *I-V* measurement. The data logging system (Agilent 34970A data acquisition/switch unit) was used for real time measurement of dynamic conductance of LbL assembled SWCNT multilayer resistors from initial conductance at the atmosphere to different *p*H buffer solutions.

D. Scanning electron microscopy and Fourier transform infrared spectroscopy characterization

The fabricated device was characterized with field emission gun scanning electron microscopy (SEM) (Jeol FE-SEM 6500) with an acceleration voltage of 10 kV. Prior to that, the fabricated device was sputtered with a layer of platinum 50 Å thick to enhance the surface conductivity. f-SWCNT samples for Fourier transform infrared (FTIR) spectroscopy were prepared by drop casting of SWCNT solution onto Si/SiO_2 surface cleaned as mentioned previously. The reflective Fourier transform infrared spectrometer (Nicolet Magna IR 750) was used with the background of Si/SiO_2 surface to characterize induced surface functional groups. The spectra were obtained as the absorbance in the mid-infrared region, $4000-400\ cm^{-1}$ by averaging 1000 scans with a spectral resolution of $2\ cm^{-1}$.

III. RESULTS AND DISCUSSIONS

The fabricated LbL assembled SWCNT thin-film sensor is illustrated in Fig. 1. In LbL multilayer hierarchy, as shown in Fig. 1(a), there are $(PDDA/PSS)_2$ as a precursor layer for the charge enhancement and $(PDDA/SWCNT)_5$ as an electrochemical transducer material. The spun PMMA in the outmost layer plays a role of the dielectric. The conductance behavior and *p*H sensing mechanism will be discussed in the absence and presence of the dielectric PMMA. The fabricated SWCNT thin-film sensor depicted in Fig. 1(b), was submerged into *p*H buffer solutions with a Ag/AgCl reference electrode connected to the source electrode to provide a stable potential as shown in Fig. 1(c), and the current flowing through SWCNT multilayer was acquired at the bias voltages from 0 to 1 V. The SEM images of the fabricated device are shown in Fig. 2. The source-drain electrodes along with SWCNT multilayer thin film in the channel area are shown in Fig. 2(a). The dimension of sensing channel used in this study is 10 μm long and 1 mm wide. The surface of $(PDDA/PSS)_2$ $(PDDA/SWCNT)_5$ is illustrated in Fig. 2(b), where the individual SWCNTs, its bundle, and random network are clearly observed.

The chemical functionalization of pristine SWCNTs (p-SWCNT) is illustrated in Fig. 3. The reflective FTIR spectrum of f-SWCNT is shown in Fig. 3(a). The characteristic absorption peaks are observed at the wave numbers of 1740, 1580, 1150, and 1105 and the broadband of

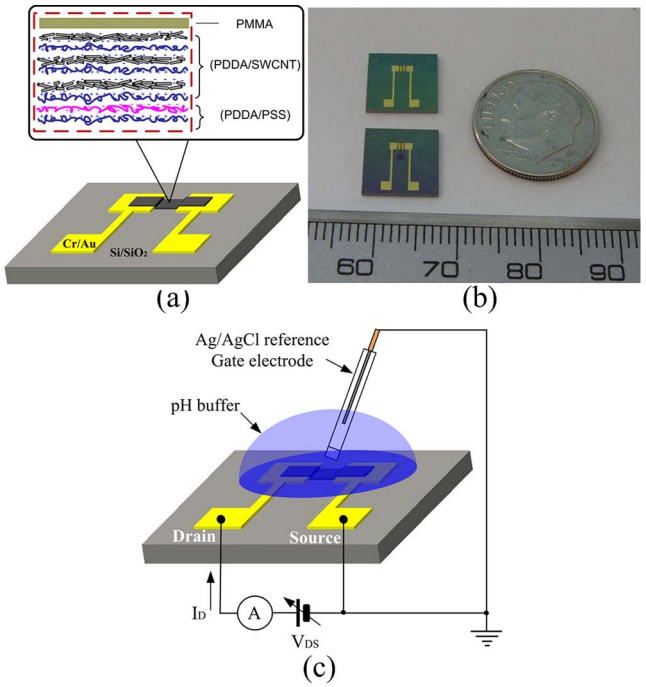

FIG. 1. (Color online) Fabricated LbL assembled SWCNT multilayer thin-film sensor: (a) schematic of multilayer hierarchy, (b) a photograph of the individual device, and (c) current-voltage (*I-V*) characteristic testing apparatus at *p*H buffers.

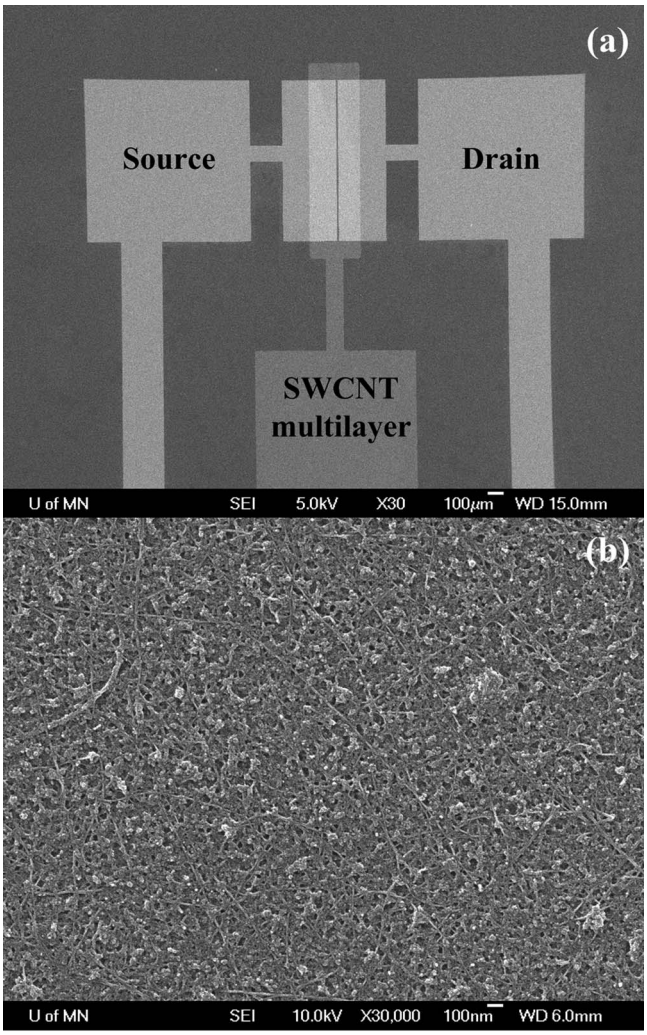

FIG. 2. SEM image of (a) source and drain electrodes along with SWCNT multilayer film and (b) SWCNT terminated surface.

3100–3500 cm^{-1}. The sharp peaks at 1740 and 1150 cm^{-1} are associated with the stretching vibration of C=O and C–O, respectively, which are considered as the obvious indication of the functionalization of SWCNTs with carboxylic groups.[17] Furthermore, the broadband on the range of 3100–3500 cm^{-1} is originated from the stretching of –OH in the carboxylic acids.[18] The peak at 1580 cm^{-1} is ascribed to the C=C stretching vibration of intrinsic SWCNTs.[17] The sharp peak found at 1105 cm^{-1} is attributed to Si–O–Si vibration of the Si/SiO_2 substrate used.[18] Gradual increases observed under the wave number of 1500 cm^{-1} is also caused by the Si wafer as a substrate. Therefore, it is obvious that carboxylic groups are materialized as a result of the chemical treatment. In addition to that, it is hypothesized that the p-SWCNTs are fragmented on the site of defects on the side wall and uncapped at both ends, where pentagon rings exist as shown in Fig. 3(b). The carboxylic functional group was equipped on both ends as well as the side wall.[19]

I-V characteristics of SWCNT multilayer sensor without PMMA layer is shown in Fig. 4. It is evident that the current decreases with *p*H increase over the bias voltage used, as indicated in Fig. 4(a), which is opposite *p*H-dependent conductance change to the reported results.[14,15] They argued that the electronic status of pristine CNTs was changed due to proximal hydrogen (H^+) or hydroxyl ions (OH^-). The *p*H-dependent conductance behavior shows entirely different tendency by grafting carboxylic groups. Moreover, considering that protonation/deprotonation occurs in the carboxylated SWCNTs when *p*H changes,[20] a comprehensive Henderson-Hasselbach equation for carboxyl group f-SWCNT can be described as follows:

$$\mathrm{SWCNT-COOH} \overset{K_a}{\Leftrightarrow} \mathrm{SWCNT-COO^- + H^+},$$

$$\frac{[\mathrm{SWCNT-COOH}]}{[\mathrm{SWCNT-COO^-}]} = 10^{pK_a - p\mathrm{H}},$$

where pK_a is the negative logarithmic value of acid dissociation constant (K_a). The exponential decaying function was fit to current values at the same bias voltage and found to be in great agreement with experimental data, as shown in Fig. 4(b). Consequently, carboxylated SWCNT behaves as a weak polyacid and the protonation/deprotonation plays an important role in shifting the conductance of SWCNTs at different *p*H buffer solutions. However, it is noted that the metallic SWCNTs that are predicted as $\frac{1}{3}$ of all SWCNTs in thin film[21] provide an offset current and an explicit relationship between $[\mathrm{SWCNT-COOH}]/[\mathrm{SWCNT-COO^-}]$ and the conductance of the SWCNT has not been reported yet. Ad-

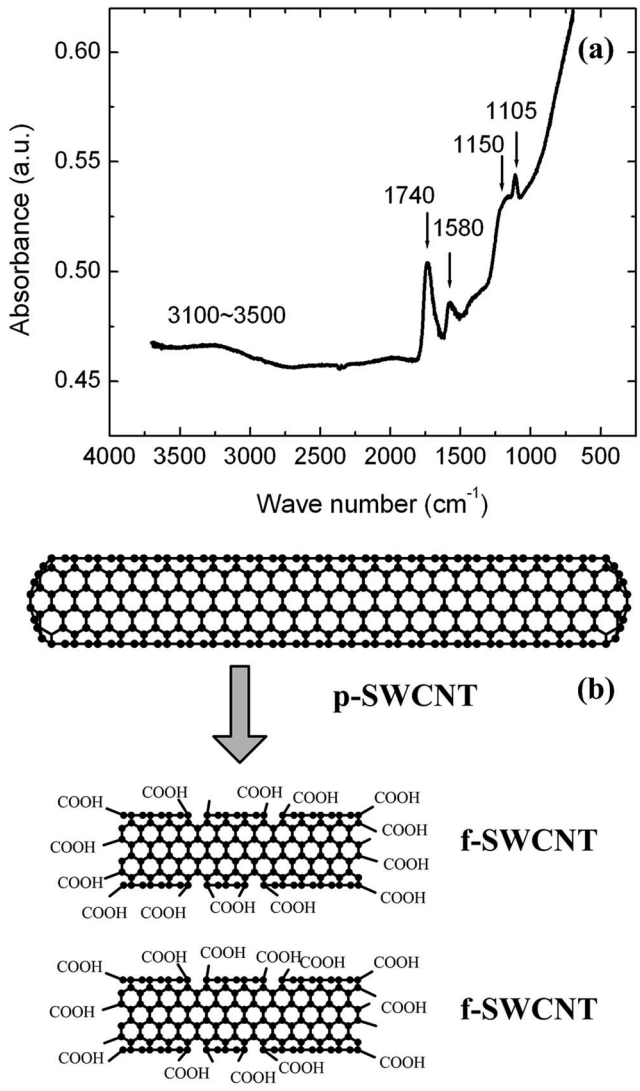

FIG. 3. Chemical functionalization of p-SWCNT by concentrated acid treatment: (a) reflective FTIR spectrum of the f-SWCNT and (b) schematic process of chemical functionalization.

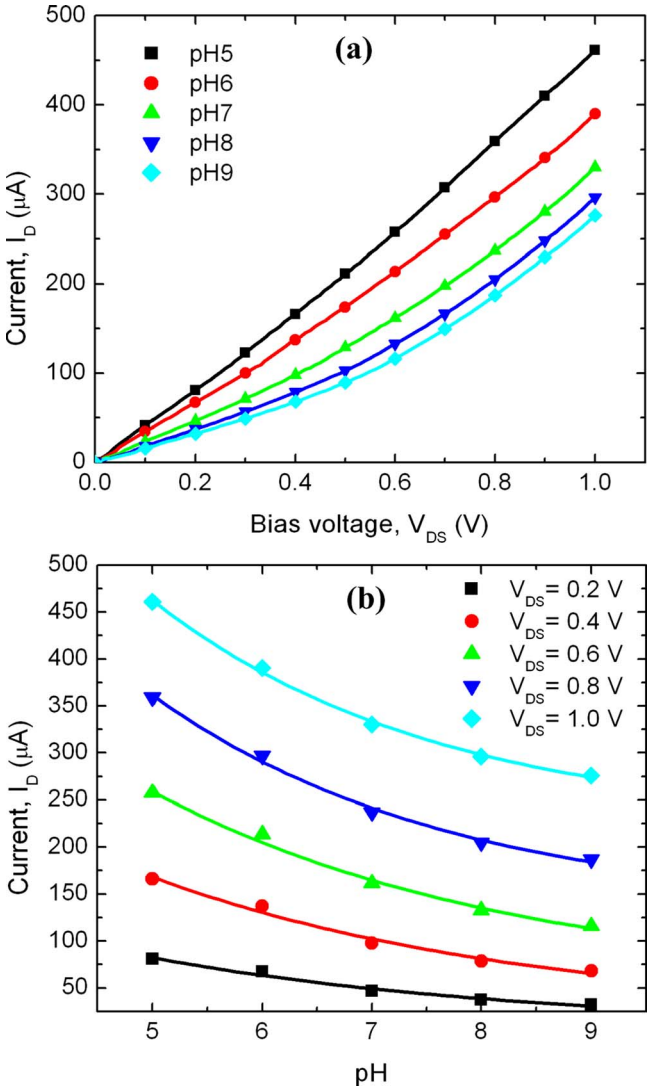

FIG. 4. (Color online) *I-V* characteristics of SWCNT multilayer thin-film sensors at different *p*H buffer solutions (a) and *p*H-dependent conductance change (b) in the absence of PMMA.

ditionally, the reason for parabolic behavior in the current over the bias voltage in each *p*H buffer, as shown in Fig. 4(a), is that the ionic conductor plays an important role in the higher bias voltage by driving salt and its counterions to flow between source and drain electrodes.

On the ground that the carboxylated SWCNT is a *p*-type semiconductor[22] protonation/deprotonation can be interpreted as the hole doping/undoping from the solid-state semiconductor perspectives in the absence of PMMA layer. This hypothetical model is illustrated in Fig. 5, where protonation/deprotonation of carboxylic groups on the surface of SWCNT is considered as hole doping/undoping as charge carriers. As a result, the conductance of SWCNT reflects the collective protonation/deprotonation status of all carboxylic groups on the SWCNT surface.

I-V characteristics of SWCNT multilayer resistor with PMMA layer is shown in Fig. 6. As opposed to the absence of PMMA, the current increases with *p*H in the presence of PMMA dielectric layer, as shown Fig. 6(a). Even though the sensitivity is significantly decreased, a linear dependence of the current on bias voltage in each *p*H buffer is observed, which means that the ionic conductor is passivated by PMMA spin coating. Importantly, it is considered that the difference in $[H^+]$ between the inside and outside PMMA layer plays a role of the gate voltage due to Nernst potential as follows:

$$V_{H^+} = C \log\left(\frac{[H^+]_o}{[H^+]_i}\right),$$

where C is the proportional constant, $[H^+]_o$ is the hydrogen ion concentration outside PMMA, which is determined by *p*H of bulk sample solution, and $[H^+]_i$ is the hydrogen concentration inside PMMA. By passivating the hydrogen ions penetration, the *p*H increase in bulk *p*H buffer solution is equivalent to a negative gate bias from conventional FETs. Therefore, the conductance of SWCNT multilayer thin-film

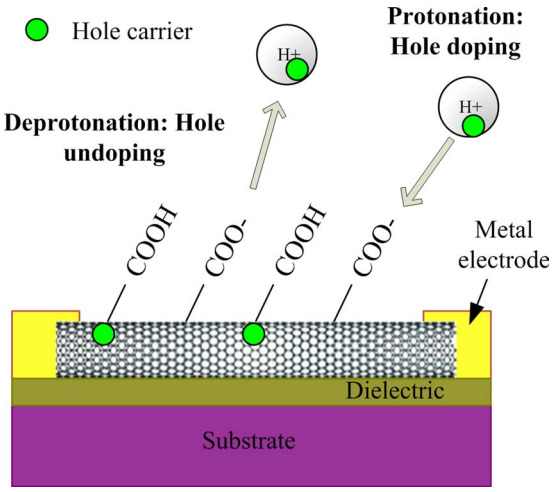

FIG. 5. (Color online) Hypothetical model of the conductance shift in carboxylated SWCNT by means of protonation/deprotonation from solid-state semiconductor perspectives.

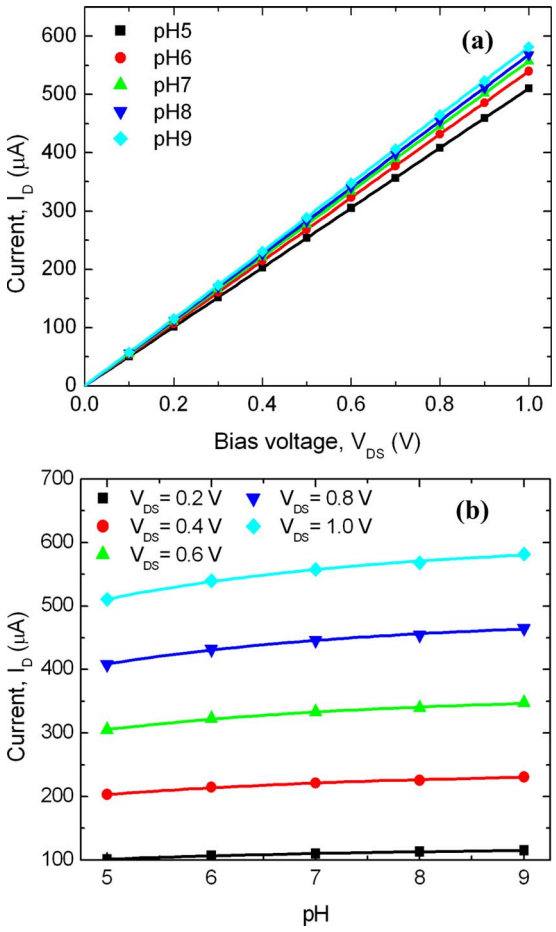

FIG. 6. (Color online) *I-V* characteristics of SWCNT multilayer resistor at different *p*H buffer solutions (a) and *p*H-dependent conductance change (b) in the presence of PMMA layer as a dielectric.

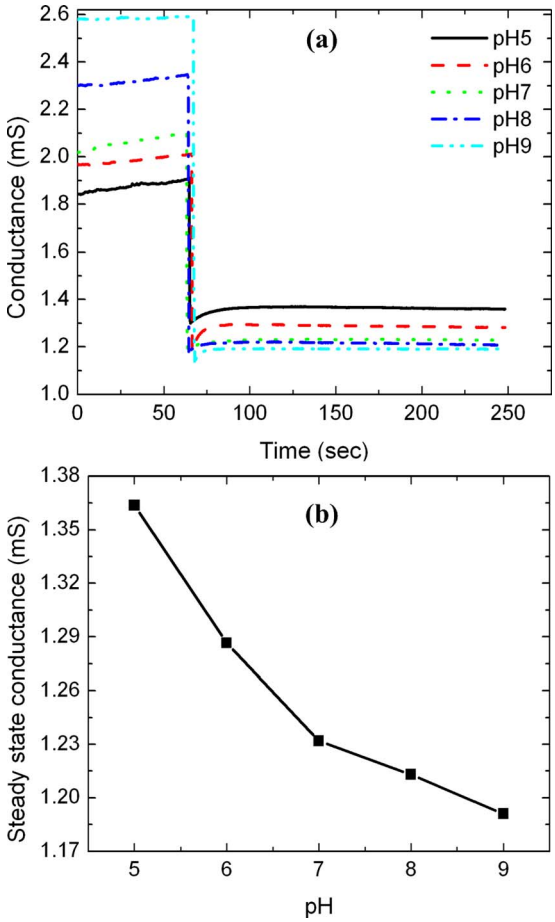

FIG. 7. (Color online) Time responses of the conductance change of SWCNT multilayer resistor (a) and steady state conductance at difference *p*H buffer solutions (b) in the absence of PMMA layer.

resistor is enhanced as *p*H increases[10] in the presence of PMMA layer, as shown in Fig. 6(b). The main chemical change in PMMA by *p*H driven hydrolysis of ester groups happens at terminal $-O-CH_3$ groups, which changes to –OH and $-O^-$ in acidic and basic environment, respectively.[23] In this case, cleavage of PMMA backbone chain does not happen. Consequently, the surface charge induced by the hydrolysis of ester groups in PMMA reinforces the effect of membrane gate potential induced by bulk *p*H solution. In acidic, H^+ ions are pulled to monomer terminal groups, which gives constricted hydrogen ion concentrations, whereas negative charges are induced in basic solutions. Therefore, the surface charge induced in PMMA can boost up gate potential effects in ion-sensitive FET (ISFET) sensors.

The time responses of SWCNT multilayer sensors in the absence and presence of PMMA layer are illustrated in Figs. 7 and 8, respectively. The same device was used to characterize dynamic responses at each *p*H buffer with intermediate rinsing with DIH_2O, followed by drying. The initial conductance difference was substantially observed in the atmosphere, before corresponding *p*H buffer was applied in both batches of sensors as shown in Figs. 7(a) and 8(a). After the application of *p*H buffers at the elapsed time of 1 min, the

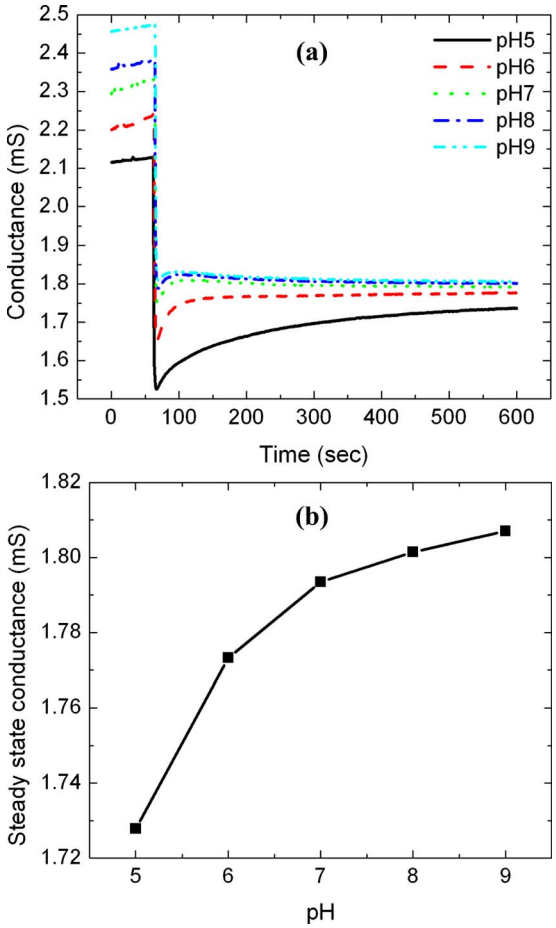

FIG. 8. (Color online) Time responses of the conductance change in SWCNT multilayer resistor (a) and steady state conductance at different *p*H buffer solutions (b) in the presence of PMMA layer.

conductance was significantly decreased and stabilized within 10 and 30 s as shown in Figs. 7(a) and 8(a), respectively. The abrupt reduction in conductance is primarily caused either by the decrease in interconnection of SWCNTs due to swelling or the surface wetting of the SWCNT thin film. Compared to relatively stable signal in the buffer solutions, the substantial drift in the atmosphere was caused primarily by the wetting and dry status of the SWCNT multilayer thin-film surface and by ambient air flow. The conductance was increased with the time after the intermediate washing since the moisture was evaporated. In addition, the reference electrode could not play a role of providing a stable potential without any buffer solutions. Without PMMA layer, in Fig. 7(b) the steady state conductance decreases exponentially with increase in *p*H, which is in good agreement with *I-V* characteristics shown in Fig. 4(b). On the other hand, the conductance with PMMA layer increases with *p*H, which is also consistent with *I-V* curve in Fig. 6(b).

IV. CONCLUSION

In conclusion, we have demonstrated *p*H-dependent conductance responses of LbL assembled polyelectrolytes and carboxylated SWCNT multilayer thin-film resistors and elucidated the mechanism of conductance change depending on *p*H in the absence and presence of PMMA dielectric layer. In the case of the sensors without PMMA as an isolation layer, the conductance decreases exponentially with increase in *p*H. This is justified by hole doping/undoping as charge carriers to *p*-type semiconducting SWCNTs by means of molecular protonation/deportation. This tendency is completely different from the previously reported results,[14,15] where pristine SWCNT was used. The different tendencies can be attributed to the presence of carboxylic groups on the SWCNTs, having the weak polyacid behavior. In the presence of PMMA as dielectric, the conductance increases with *p*H. The ionic Nernst potential across the dielectric layer plays a role of the gate potential for the *p*-type semiconducting SWCNT layer in a sense of conventional FETs. This device functions as an ISFET, where the metal gate is removed and ion concentrations act as the electrical potential. Based on the different *p*H-dependent conductance mechanisms that we have found, versatile device structures can be constructed for various applications to chemical and biological sensors detecting the reactions accompanying *p*H change.

ACKNOWLEDGMENTS

This work was partially supported by the DARPA M/NEMS Science and Technology Fundamental Research Program through the Micro/Nano Fluidic Fundamental Focus (MF3) Center. The authors would like to thank the Nanofabrication Center and Characterization Facility at the University of Minnesota for the help with fabrication and characterization.

[1] J. Han, in *Carbon Nanotubes: Science and Applications*, edited by M. Meyyappan (CRC, New York, 2005), Chap. 1, p. 8.
[2] R. Martel, T. Schmidt, H. R. Shea, T. Hertel, and Ph. Avouris, Appl. Phys. Lett. **73**, 2447 (1998).
[3] C. Hierold, A. Jungen, C. Stampfer, and T. Helbling, Sens. Actuators, A **136**, 51 (2007).
[4] R. Krupke, F. Hennrich, H. Löhneysen, and M. M. Kappes, Science **301**, 344 (2003).
[5] T. Dürkop, S. A. Getty, E. Cobas, and M. S. Fuhrer, Nano Lett. **4**, 35 (2004).
[6] Y. A. Tarakanov and J. M. Kinaret, Nano Lett. **7**, 2291 (2007).
[7] K. Gong, Y. Yan, M. Zhang, L. Su, S. Xiong, and L. Mao, Anal. Sci. **21**, 1383 (2005).
[8] A. Star, J.-C. P. Gabriel, K. Bradley, and G. Grüner, Nano Lett. **3**, 459 (2003).
[9] X. Tang, S. Bansaruntip, N. Nakayama, E. Yenilmez, Y.-L. Chang, and Q. Wang, Nano Lett. **6**, 1632 (2006).
[10] M. Lu, D. Lee, W. Xue, and T. Cui, in Proceedings of the 21st IEEE International Conference on Micro Electro Mechanical Systems, MEMS 2008 Technical Digest, edited by O. Brand and Y. Zohar (IEEE, Piscataway, NJ, 2008), p. 188–191.
[11] H. Boo *et al.*, Anal. Chem. **78**, 617 (2006).
[12] J. Wang, M. Li, Z. Shi, N. Li, and Z. Gu, Anal. Chem. **74**, 1993 (2002).
[13] C.-F. Lin, G.-B. Lee, C.-H. Wang, H.-H. Lee, W.-Y. Liao, and T.-C. Chou, Biosens. Bioelectron. **21**, 1468 (2006).
[14] J. H. Back and M. Shim, J. Phys. Chem. B **110**, 23736 (2006).
[15] J. Kwon, K. Lee, Y. Lee, and B. Ju, Electrochem. Solid-State Lett. **9**, H85 (2006).
[16] Y. Liu and T. Cui, Sens. Actuators B **123**, 148 (2007).
[17] D. S. Bag, R. Dubey, N. Zhang, J. Xie, V. K. Varadan, D. Lal, and G. N. Mathur, Smart Mater. Struct. **13**, 1263 (2004).
[18] G. Gauglitz and T. Vo-Dinh, *Handbook of Spectroscopy* (Wiley, Weinheim, 2002), Vol. 1.

[19]J. Liu *et al.*, Science **280**, 1253 (1998).
[20]W. Zhao, C. Song, and P. E. Pehrsson, J. Am. Chem. Soc. **124**, 12418 (2002).
[21]T. Dürkop, B. M. Kim, and M. S. Fuhrer, J. Phys.: Condens. Matter **16**, R553 (2004).
[22]W. Xue, Y. Liu, and T. Cui, Appl. Phys. Lett. **89**, 163512 (2006).
[23]T. W. G. Solomons, *Organic Chemistry* (Wiley, New York, 1984), Chap. 18, p. 794.